Electrocatalysis

DOI: 10.1002/anie.201303197

Cobalt Molybdenum Oxynitrides: Synthesis, Structural Characterization, and Catalytic Activity for the Oxygen Reduction Reaction**

*Bingfei Cao, Gabriel M. Veith, Rosa E. Diaz, Jue Liu, Eric A. Stach, Radoslav R. Adzic, and Peter G. Khalifah**

Owing to energy efficiency demands, tremendous research efforts have been focused on developing efficient catalysts for proton-exchange membrane fuel cells (PEMFCs) and anion-exchange membrane fuel cells (AMFCs). Compared to hydrogen oxidation catalysis, it is much more challenging to develop suitable catalysts for the oxygen reduction reaction (ORR), as the ORR is a complex four-electron process that typically has sluggish kinetics that require high overpotentials to overcome.[1] Platinum supported on carbon is the best known cathode catalyst for ORR with a moderate overpotential (about 300 mV). However, Pt is expensive and is sensitive to contaminants such as halides, methanol, and carbon monoxide.[1] It is highly desirable to investigate non-noble-metal-based materials as alternative cathode catalysts. Various non-noble-metal catalysts (NNMCs), such as transition-metal chacogenides,[2] macrocycles,[3–5] transition-metal oxides,[6] transition-metal carbides/nitrides,[7–9] and transition-metal oxynitrides,[10–13] have been widely studied. Among these NNMCs, catalysts containing cobalt or iron have shown the most promising catalytic activities for ORR.[4,5] These highly active catalysts can be obtained by choosing the right combination of metal–nitrogen–carbon precursors and heating conditions. For example, PANI-FeCo-C was recently reported to exhibit high ORR activity with an onset potential of 0.93 V and retention of activity for 30000 cycles in a PEMFC.[5]

Transition-metal nitrides and oxynitrides are well suited for catalysis applications as they have good electrical conductivities and corrosion resistance. Their activities in hydrodenitrogenation and hydrodesulfurization resemble those of noble metals.[7] The formation of nitrides favorably modifies the catalyst electronic structure such that the contraction of d-bands in Group 4–6 nitrides results in a greater electron density near Fermi level. This facilitates the donation of electrons to adsorbates such as oxygen.[7] Therefore, the formation of nitrides on the surface may make it easier for the catalytically active metal to reduce oxygen. Previously, ORR activities of monometallic nitrides/oxynitrides of Group 4–6 have been studied in acidic solution for fuel-cell applications.[7–11] ZrO_xN_y and TaO_xN_y were found to show moderate ORR activities and excellent chemical stabilities in sulfuric acid.[10,11] Studies on MoN and Mo_2N demonstrated that they had comparatively good ORR activities and that the oxygen reduction reaction proceeds through a nearly four-electron process.[8,9] Compared to monometallic oxynitrides, bimetallic oxynitrides are potentially better ORR catalyst candidates since their catalytic properties can be enhanced by the combination of multiple active species or by the tuning of electronic states. Indeed, bimetallic Co-W-O-N catalysts supported on carbon were found to have an onset potential of 0.749 V in 0.5 M H_2SO_4, an activity substantially higher than monometallic W and Co oxynitrides.[12] Oyama et al. have synthesized bimetallic oxynitrides Co-Mo-O-N with high surface areas that showed excellent hydrodenitrogenation activities.[14] Similar to Co-W-O-N, we hypothesized that Co-Mo-O-N may possess good ORR activities as well. Herein, we report the synthesis and characterization of $Co_xMo_{1-x}O_yN_z$ compounds supported on carbon black as effective catalysts for ORR in acidic media and as exceptional ORR catalysts in basic environments.

Catalyst powders with nominal compositions of $Co_xMo_{1-x}O_yN_z$ were purchased ($x = 1.0$, CoO) or synthesized ($x = 0.0$, 0.25, 0.50, and 0.75) with soluble cation precursors, which were precipitated and then reacted under flowing ammonia at low temperatures (773–973 K) with the goal of producing cubic rock salt products. Temperatures and reaction times were optimized to minimize the amount of reaction side-products (typically Co metal or Co_3Mo_3N). X-ray

[*] B. Cao, J. Liu, Prof. P. G. Khalifah
Chemistry Department, Stony Brook University
Stony Brook, NY 11794 (USA)
E-mail: kpete@bnl.gov
Dr. G. M. Veith
Material Science and Technology Division
Oak Ridge National Laboratory, Oak Ridge, TN 37831 (USA)
Dr. R. E. Diaz, Dr. E. A. Stach
Center for Functional Nanomaterials
Brookhaven National Laboratory, Upton, NY 11793 (USA)
Dr. R. R. Adzic, Prof. P. G. Khalifah
Chemistry Department
Brookhaven National Laboratory, Upton, NY 11793 (USA)

[**] This work was carried out at BNL under Contract DEAC02-98CH10886 with the U.S. Department of Energy, both in the Chemistry Department and in the Center for Functional Nanomaterials user facility. Primary funding was provided by BNL LDRD 10-0012 (P.G.K., R.R.A.). Acknowledgement is made to the Donors of the American Chemical Society Petroleum Research Fund for partial support of this research (P.G.K.). Research was partially supported by the U.S. Department of Energy, Basic Energy Sciences, Materials Sciences and Engineering Division (GMV). We thank Nebojsa Marinkovic and Syed Khalid for on-site assistance in using X19A beamline at National Synchrotron Light Source, Brookhaven National Laboratory.

Supporting information for this article is available on the WWW under http://dx.doi.org/10.1002/anie.201303197.

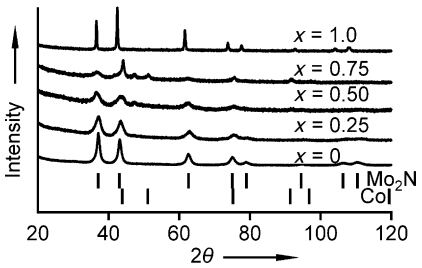

Figure 1. XRD patterns of $Co_xMo_{1-x}O_yN_z$/C synthesized at 823 K. x = Co/(Co+Mo).

diffraction (XRD) patterns of reaction products at 823 K (Figure 1) showed that the rock salt phase $Co_xMo_{1-x}O_yN_z$ was present for all of the mixed compositions studied. A substantial amount of Co metal is seen for $x = 0.75$, less for the $x = 0.50$ phase, and none for $x = 0.25$. The phase Co_3Mo_3N was observed at temperatures of 873 K and higher (Supporting Information, Figure S1). The cubic lattice parameter and the primary particle size obtained from Le Bail whole-pattern fitting (WPF; Supporting Information, Table S1) indicate that the cell volume decreases with decreasing Co content as expected for solid solution formation, though Mo_2N is an outlier from this trend. Based on WPF data, the primary particle size is about 10 nm for Mo_2N and 4–5 nm for the bimetallic samples, which is substantially lower than the 30 nm of the purchased CoO.

The ORR activity of carbon-supported $Co_xMo_{1-x}O_yN_z$ compounds was assessed by cyclic voltammetry (CV) and rotating disk electrode (RDE) measurements. First, the acidic ORR activities of samples of $Co_{0.50}Mo_{0.50}O_yN_z$ (nominal composition) that had been treated at different temperatures were compared (Supporting Information, Figure S2a). The best activity was obtained for the sample treated at 823 K, which had an onset potential of 0.645 V vs. RHE and reached a current density of 4.1 mA cm^{-2} at 0.20 V vs. RHE in RDE measurements (Supporting Information, Table S2); this value is close to the diffusion-limited current density expected for a four-electron pathway.[2] The ORR activities rapidly drop for samples treated at 873 K and above. The 923 K sample was phase-pure Co_3Mo_3N, which can clearly be seen to be inactive for ORR electrocatalysis. Composition also impacts ORR performance (Figure 2; Supporting Information, Table S3). The bimetallic oxynitride $Co_{0.50}Mo_{0.50}O_yN_z$ had substantially better activities than binary Mo_2N and CoO,

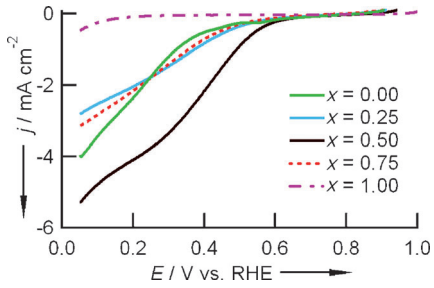

Figure 2. RDE curves of $Co_xMo_{1-x}O_yN_z$/C with different Co/Mo ratios synthesized at 823 K, measured in O_2-saturated 0.1 M $HClO_4$.

which suggests that Co substitution into Mo_2N enhanced its activity for acidic ORR by about 0.2 V. $Co_{0.75}Mo_{0.25}O_yN_z$/C and $Co_{0.25}Mo_{0.75}O_yN_z$/C both exhibited ORR activity, though at a rate only slightly higher than that of Mo_2N. The activity of $Co_{0.50}Mo_{0.50}O_yN_z$ is substantially better than reported ZrO_xN_y[10] and TaO_xN_y,[11] whose current densities were only about 50 μA cm^{-2} at 0.4 V, which is far lower than the 3 mA cm^{-2} measured for $Co_{0.5}Mo_{0.5}O_yN_z$ at the same voltage.

The $Co_{0.50}Mo_{0.50}O_yN_z$/C catalyst has a moderate activity that is better than that of binary Mo_2N but is lower than that of Pt, as seen in its Tafel slope (Supporting Information, Figure S2b) of −160 mV/dec, a value significantly larger than that of Pt/C (−87 mV/dec). RDE measurements of $Co_{0.50}Mo_{0.50}O_yN_z$/C (823 K) in $HClO_4$ (Supporting Information, Figure S3a) were carried out to study its ORR kinetics. At low potential ranges, both two- and four-electron reductions take place with a calculated number n of 3.6 transferred electrons from Koutecky–Levich analysis at potentials below 0.35 V vs. RHE. Rotating ring disk electrode (RRDE) measurement confirm a mixed mechanism, as seen in the peroxide yield of 30–40 % between 0.1 to 0.3 V and the deduced n of about 3.2 (Supporting Information, Figure S3b).

Although $Co_xMo_{1-x}O_yN_z$/C samples have moderate activity in acid, they are exceptionally active in alkaline conditions (pH 13). Both synthesis temperature and composition impact activity (Figure 3; Supporting Information, Tables S4, S5). The highest activity is achieved by $Co_{0.50}Mo_{0.50}O_yN_z$/C (823 K)

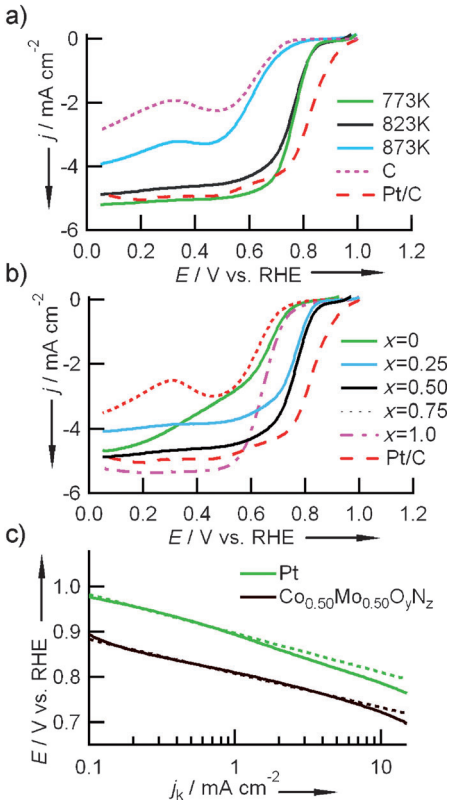

Figure 3. In 0.1 M KOH saturated with O_2: a) RDE curves of $Co_{0.50}Mo_{0.50}O_yN_z$/C treated between 773 K and 923 K. b) RDE curves of $Co_xMo_{1-x}O_yN_z$/C with different Co/Mo ratios. c) Tafel plots of $Co_{0.50}Mo_{0.50}O_yN_z$/C (823 K) and Pt/C derived from RDE data.

with an onset potential as high as 0.918 V vs. RHE and an E_{half} of 0.758 V. This is only about 0.1 V lower than commercial Pt/C samples (Etek) measured under the same conditions here and elsewhere.[2] Among the various non-noble metal systems studied under basic conditions, only perovskite $LaNiO_3$ is clearly better than $Co_{0.50}Mo_{0.50}O_yN_z$/C based on a comparison of onset potentials and currents at fixed potential (Supporting Information, Table S6). The diffusion-limited current density of $Co_{0.50}Mo_{0.50}O_yN_z$/C is about 4.8 mA cm^{-2}, which is very close to that of Pt (5.0 mA cm^{-2}). Above 0.8 V vs. RHE, the Tafel slope is −71 mV/decade (Figure 3c), which is smaller than of Pt/C (−87 mV/dec).

Analysis of Koutecky–Levich plots at potentials of 0.4–0.7 V vs. RHE (Figure 4) gave $n = 3.85$, indicating a four-electron pathway is the dominant mechanism. RRDE data demonstrated that only 2–4% peroxide was produced, giving $n = 3.9$. Durability testing of $Co_{0.50}Mo_{0.50}O_yN_z$/C (823 K) indicates that the sample retains activity during extended testing in both alkaline (24 h at a potential of 0.6 V) and acidic (40 h at a potential of 0.4 V) environments (Supporting Information, Figure S4).

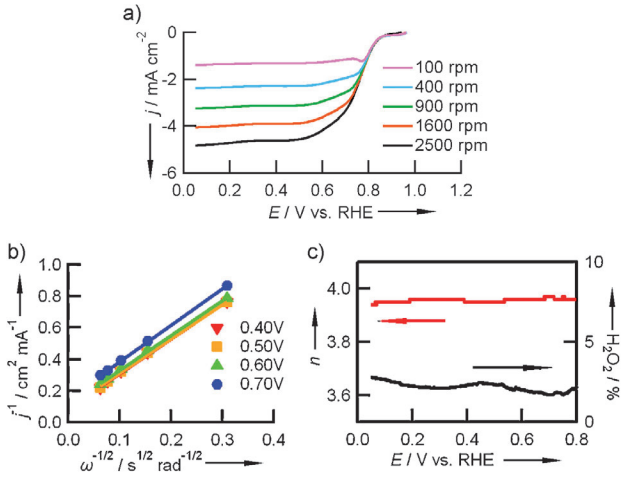

Figure 4. In 0.1 M KOH saturated with O_2: a) RDE curves of $Co_{0.50}Mo_{0.50}O_yN_z$/C (823 K) with a rotation speed of 100–2500 rpm. b) Koutechy–Levich plot at a potential range of 0.40 to 0.70 V vs. RHE. c) Percentage of peroxide and the electron-transfer number of $Co_{0.50}Mo_{0.50}O_yN_z$/C (823 K) based on the RRDE data.

The ORR results show that the bimetallic composition of $Co_xMo_{1-x}O_yN_z$ can strongly enhance ORR activity. Bulk XRD data (Figure 1) revealed that this sample contains metallic Co and its true stoichiometry is likely Mo-rich relative to the nominal stoichiometry. Comprehensive measurements were carried out to probe the actual composition of the rock salt phase in nominal $Co_{0.50}Mo_{0.50}O_yN_z$ and to better understand its bulk and atomic-scale structure. Scanning electron microscopy (SEM, Figure 5a) showed that $Co_{0.50}Mo_{0.50}O_yN_z$ is composed of 0.3–1.0 μm particles with surface nanoparticles (20–30 nm) of Co metal, an acid-soluble species which can be removed by washing with perchloric acid (Supporting Information, Figure S5). Energy-dispersive X-ray spectroscopy (EDX) studies find abundant oxygen and

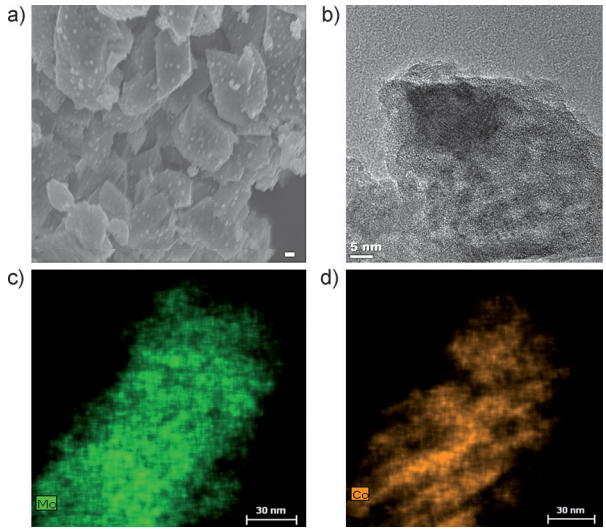

Figure 5. a) SEM image of $Co_{0.50}Mo_{0.50}O_yN_z$ (823 K) with smaller surface Co nanoparticles. Scale bar: 100 nm. b) TEM image of $Co_{0.50}Mo_{0.50}O_yN_z$ (823 K) showing inhomogeneity on a 5 nm scale. Scale bar: 5 nm. c) STEM-EDX map of Mo distribution. Scale bar: 30 nm. d) STEM-EDX map of Co distribution. Scale bar: 30 nm.

nitrogen in the rock salt phase, confirming that it is indeed an oxynitride.

Given the large particle size of the rock-salt phase in SEM experiments, it is surprising that the X-ray coherence length observed for $Co_{0.50}Mo_{0.50}O_yN_z$ (823 K) was only about 5 nm. More local TEM studies find that sample heterogeneity exists for even the smallest rock-salt particles (ca. 25 nm). When the thin edge regions of particles were observed, it could be clearly seen that they presented a heterogeneous morphology on a length scale of about 5 nm (Figure 5b), which is attributed to sample porosity arising from the reductive elimination (by evaporation) of cobalt metal during processing under reducing conditions (NH_3 flow). STEM-EDX maps clearly show that Mo is distributed evenly throughout particles, but that there are Co-rich clusters in their interior attributed to Co metal inclusions (Figures 5c and d). Co loss from the exterior of particles is also seen in electron energy loss spectroscopy (EELS) line scan analyses (Supporting Information, Figure S6). These scans find Co even outside of the Co-rich clusters, thus confirming that the rock salt phase is a true bimetallic compound.

The valence states of Co and Mo in bulk $Co_xMo_{1-x}O_yN_z$ were analyzed using X-ray absorption near-edge spectroscopy (XANES). As seen in Figure 6a, three characteristic features are present in the Co K-edge spectra: a pre-edge peak (ca. 7709 eV), an edge jump (ca. 7717 eV), and a white line (ca. 7725 eV).[15] There is a striking similarity between the patterns of $Co_{0.50}Mo_{0.50}O_yN_z$ and $Co_{0.25}Mo_{0.75}O_yN_z$, suggesting that the Co environments in these samples are very similar. XANES data for $Co_{0.50}Mo_{0.50}O_yN_z$ and $Co_{0.25}Mo_{0.75}O_yN_z$ do not exhibit the isosbestic points that would be expected from a simple mixture of Co metal and CoO, indicating that the catalytically active phase is indeed a distinct bimetallic rock salt compound. In the Mo $L_{2,3}$ edge spectra, $Co_{0.50}Mo_{0.50}O_yN_z$ and

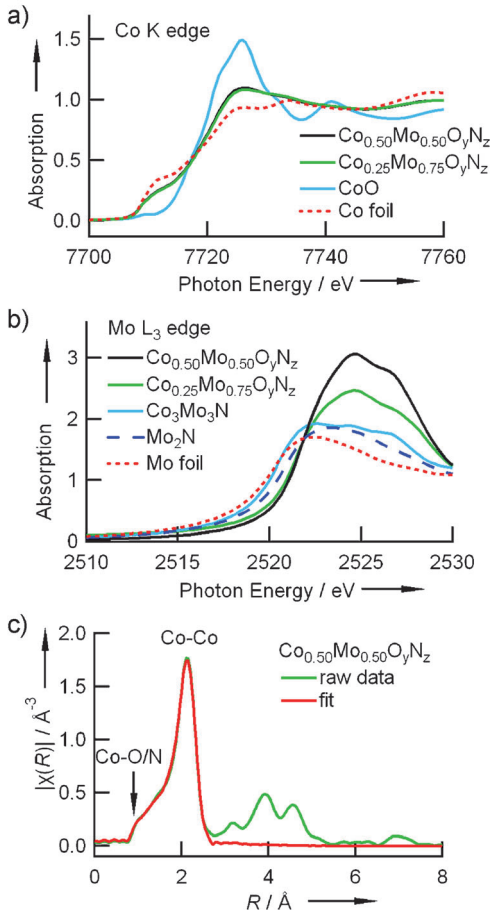

Figure 6. XAFS studies of the most active $Co_{0.50}Mo_{0.50}O_yN_z$/C sample. a) XANES spectra near the Co K-edge, indicating a mix of metallic and divalent Co. b) XANES spectra near the Mo L_3-edge, demonstrating that the Mo valence is slightly higher than in Mo_2N. c) Co K-edge EXAFS (green) spectrum with fit (red) to a mixture of Co metal and Co–O/N bonds over the first coordination shell (to ca. 2.5 Å).

$Co_{0.25}Mo_{0.75}O_yN_z$ have a similar Mo environment (Figure 6b). The oxidation state of Mo in these two compounds is clearly higher than that in the reference compounds Co_3Mo_3N and Mo_2N, and is highest for the $Co_{0.50}Mo_{0.50}O_yN_z$ sample with the highest activity. The splitting of the white line around 2525 eV indicates that Mo may have an octahedral environment in these oxynitrides,[16] as would be expected for the rock salt structure.

An extended X-ray absorption fine structure (EXAFS) study of the Co K-edge can clearly distinguish between coordination environments of Co metal and ionic Co. Fitting was carried out for the first coordination shell (Figure 6c; Supporting Information, Figure S7), which was modeled using Co–Co and Co–O paths. The calculated bond lengths between cobalt and anion for both samples (Supporting Information, Table S7) are consistent with those deduced from the lattice parameters obtained from Le Bail fits of X-ray diffraction data. The EXAFS data for both $Co_{0.50}Mo_{0.50}O_yN_z$ and $Co_{0.25}Mo_{0.75}O_yN_z$ show a strong peak at about 2.48 Å indicative of the Co–Co bonding in Co metal. There is a shoulder at lower distances that can be well-fit by assuming a component with octahedral coordination of Co that refines to 55% and 66% of the Co species in the $x = 0.50$ and 0.25 samples, respectively. The true compositions are thus $Co_{0.18}Mo_{0.82}O_yN_z$ for $x = 0.25$ and $Co_{0.35}Mo_{0.65}O_yN_z$ for $x = 0.50$. It is therefore concluded that the incorporation of CoO into the rock-salt structure of Mo_2N occurs and is necessary for the enhanced ORR activity.

X-ray photoelectron spectroscopy (XPS) measurements were performed to study catalyst surface properties of both as-prepared samples and of samples after exposure to air and ORR reaction experiments (Supporting Information, Tables S8, S9). The N 1s data demonstrates that there are significant concentrations of nitrogen species near the surface for all samples (Supporting Information, Figure S8). The Co $2p_{3/2}$ data exhibits a dominant peak at 781.6 eV owing to Co–O or Co–N species, consistent with bulk EXAFS results. The Mo 3d XPS data is consistent with XPS data reported for other molybdenum nitrides,[17] with major peaks located at about 229 eV, which is due to $Mo^{2/3+}$, 230 eV, for $Mo^{3/4+}$, and 232.8 eV, for Mo^{6+}. XPS indicated that the top few nanometers of $Co_{0.50}Mo_{0.50}O_yN_z$/C and $Co_{0.25}Mo_{0.75}O_yN_z$/C samples contained about 20 at% $Mo^{2/3+}$, 30 at% $Mo^{3/4+}$, and 50 at% Mo^{6+}. This ratio remained essentially unchanged after air exposure, indicating that the reduced Mo species are quite stable. Interestingly, the $Co_{0.50}Mo_{0.50}O_yN_z$/C sample produced at 773 K, contained only $Mo^{3/4+}$ (42 at%) and Mo^{6+} (58 at%) and no evidence of the lowest oxidation state $Mo^{2/3+}$ species. This Mo data, along with the Co 2p data, indicates reactions at higher temperatures lead to a preferential reduction in the Mo valence on the electrode surface; Co seems unaffected and remains divalent. The $Co_{0.50}Mo_{0.50}O_yN_z$/C sample prepared at 823 K with $Mo^{2/3+}$ performs better than the 773 K sample without $Mo^{2/3+}$, suggesting that the higher Mo oxidation state may be linked to the enhanced electrochemical activity of this rock salt phase. It is anticipated that there are viable substitutional strategies, which (like elevated temperature processing) will give an optimal Mo valence at the catalytically active surface and provide new routes for further increasing the activity of this system.

In conclusion, non-noble $Co_xMo_{1-x}O_yN_z$/C catalysts synthesized by a solution impregnation method followed by ammonolysis exhibit moderate ORR activity in acidic conditions and superb activity in alkaline conditions, which is only 0.1 V away from the performance of Pt/C. Samples of nominal composition $Co_{0.50}Mo_{0.50}O_yN_z$/C treated at 823 K demonstrated the best activity ($E_{onset} = 0.918$ V vs. RHE in base and $E_{onset} = 0.645$ V vs. RHE in acid) and a four-electron or nearly four-electron pathway for ORR in both media. Although some cobalt metal is invariably formed during syntheses, ionic cobalt was demonstrated to be integrally substituted into the rock-salt structure to form a bimetallic cobalt molybdenum oxynitride with nanoscale (ca. 5 nm) texture that is catalytically active for oxygen reduction. It is suggested that strategies for tuning the metal oxidation states within the oxynitride phase are likely to lead to further enhancements in ORR activity with the potential of matching or exceeding the activity of Pt.

Received: April 16, 2013
Revised: June 5, 2013
Published online: August 28, 2013

Keywords: electrochemistry · heterogeneous catalysis · nanoparticles · oxygen reduction · oxynitrides

[1] V. Stamenkovic, B. S. Mun, K. J. J. Mayrhofer, P. N. Ross, N. M. Markovic, J. Rossmeisl, J. Greeley, J. K. Norskov, *Angew. Chem.* **2006**, *118*, 2963 – 2967; *Angew. Chem. Int. Ed.* **2006**, *45*, 2897 – 2901.
[2] H. L. Wang, Y. Y. Liang, Y. G. Li, H. J. Dai, *Angew. Chem.* **2011**, *123*, 11161 – 11164; *Angew. Chem. Int. Ed.* **2011**, *50*, 10969 – 10972.
[3] R. L. Liu, C. von Malotki, L. Arnold, N. Koshino, H. Higashimura, M. Baumgarten, K. Mullen, *J. Am. Chem. Soc.* **2011**, *133*, 10372 – 10375.
[4] F. Jaouen, J. Herranz, M. Lefevre, J. P. Dodelet, U. I. Kramm, I. Herrmann, P. Bogdanoff, J. Maruyama, T. Nagaoka, A. Garsuch, J. R. Dahn, T. Olson, S. Pylypenko, P. Atanassov, E. A. Ustinov, *ACS Appl. Mater. Interfaces* **2009**, *1*, 1623 – 1639.
[5] G. Wu, K. L. More, C. M. Johnston, P. Zelenay, *Science* **2011**, *332*, 443 – 447.
[6] J. Suntivich, H. A. Gasteiger, N. Yabuuchi, H. Nakanishi, J. B. Goodenough, Y. Shao-Horn, *Nat. Chem.* **2011**, *3*, 647 – 647.
[7] D. J. Ham, J. S. Lee, *Energies* **2009**, *2*, 873 – 899.
[8] H. X. Zhong, H. M. Zhang, G. Liu, Y. M. Liang, J. W. Hu, B. L. Yi, *Electrochem. Commun.* **2006**, *8*, 707 – 712.
[9] D. G. Xia, S. Z. Liu, Z. Y. Wang, G. Chen, L. J. Zhang, L. Zhang, S. Q. Hui, J. J. Zhang, *J. Power Sources* **2008**, *177*, 296 – 302.
[10] S. Doi, A. Ishihara, S. Mitsushima, N. Kamiya, K. I. Ota, *J. Electrochem. Soc.* **2007**, *154*, B362 – B369.
[11] A. Ishihara, K. Lee, S. Doi, S. Mitsushima, N. Kamiya, M. Hara, K. Domen, K. Fukuda, K. Ota, *Electrochem. Solid-State Lett.* **2005**, *8*, A201 – A203.
[12] T. Ando, S. Izhar, H. Tominaga, M. Nagai, *Electrochim. Acta* **2010**, *55*, 2614 – 2621.
[13] M. Chisaka, Y. Suzuki, T. Iijima, Y. Sakurai, *J. Phys. Chem. C* **2011**, *115*, 20610 – 20617.
[14] C. C. Yu, S. Ramanathan, S. T. Oyama, *J. Catal.* **1998**, *173*, 1 – 9.
[15] N. Li, X. M. Wang, S. Derrouiche, G. L. Haller, L. D. Pfefferle, *ACS Nano* **2010**, *4*, 1759 – 1767.
[16] J. A. Rodriguez, S. Chaturvedi, J. C. Hanson, A. Albornoz, J. L. Brito, *J. Phys. Chem. B* **1998**, *102*, 1347 – 1355.
[17] K. Hada, M. Nagai, S. Omi, *J. Phys. Chem. B* **2001**, *105*, 4084 – 4093.

